Comparison of Global Cerebral Blood Flow Measured by Phase-Contrast Mapping MRI With ^{15}O-H_2O Positron Emission Tomography

Mark Bitsch Vestergaard, MSc,[1]* Ulrich Lindberg, PhD,[1]
Niels Jacob Aachmann-Andersen, MD, PhD,[2] Kristian Lisbjerg, MD,[2]
Søren Just Christensen, MD,[2] Peter Rasmussen, PhD,[2]
Niels Vidiendal Olsen, MD, DMSc,[2,3] Ian Law, MD, DMSc,[4,5]
Henrik Bo Wiberg Larsson, MD, DMSc,[1,4] and Otto Mølby Henriksen, MD, PhD[5]

Purpose: To compare mean global cerebral blood flow (CBF) measured by phase-contrast mapping magnetic resonance imaging (PCM MRI) and by ^{15}O-H_2O positron emission tomography (PET) in healthy subjects. PCM MRI is increasingly being used to measure mean global CBF, but has not been validated in vivo against an accepted reference technique.
Materials and Methods: Same-day measurements of CBF by ^{15}O-H_2O PET and subsequently by PCM MRI were performed on 22 healthy young male volunteers. Global CBF by PET was determined by applying a one-tissue compartment model with measurement of the arterial input function. Flow was measured in the internal carotid and vertebral arteries by a noncardiac triggered PCM MRI sequence at 3T. The measured flow was normalized to total brain weight determined from a volume-segmented 3D T_1-weighted anatomical MR-scan.
Results: Mean CBF was 34.9 ± 3.4 mL/100 g/min measured by ^{15}O-H_2O PET and 57.0 ± 6.8 mL/100 g/min measured by PCM MRI. The measurements were highly correlated ($P = 0.0008$, $R^2 = 0.44$), although values obtained by PCM MRI were higher compared to ^{15}O-H_2O PET (absolute and relative differences were 22.0 ± 5.2 mL/100 g/min and $63.4 \pm 14.8\%$, respectively).
Conclusion: This study confirms the use of PCM MRI for quantification of global CBF, but also that PCM MRI systematically yields higher values relative to ^{15}O-H_2O PET, probably related to methodological bias.
Level of Evidence: 1

J. MAGN. RESON. IMAGING 2017;45:692–699

Measurement of cerebral blood flow (CBF) is of interest, both in the clinical setting and for research. Absolute quantification of global CBF is of key importance when investigating factors affecting the entire brain, eg, altered physiological states or aging.[1–3]

Different invasive and noninvasive methods have been used to measure global CBF.[4,5] Phase-contrast mapping (PCM) magnetic resonance imaging (MRI) allows measurement of total flow in the cerebral arteries, and calculation of global CBF by subsequently normalizing to brain volume.[6] Measurement of

View this article online at wileyonlinelibrary.com. DOI: 10.1002/jmri.25442

Received Apr 19, 2016, and in revised form Jun 22, 2016. Accepted for publication Jun 22, 2016.

*Address reprint requests to: M.B.V., Functional Imaging Unit, Department of Clinical Physiology, Nuclear Medicine and PET, Rigshospitalet, Nordre Ringvej 57, DK-2600, Glostrup, Denmark. E-mail: mark.bitsch.vestergaard@regionh.dk

From the [1]Functional Imaging Unit, Department of Clinical Physiology, Nuclear Medicine and PET, Copenhagen University Hospital Rigshospitalet Glostrup, Glostrup, Denmark; [2]Department of Neuroscience and Pharmacology, Faculty of Health Sciences, University of Copenhagen, Copenhagen, Denmark; [3]Department of Neuroanaesthesia, Neuroscience Centre, Copenhagen University Hospital Rigshospitalet Blegdamsvej, Copenhagen, Denmark; [4]Institute for Clinical Medicine, The Faculty of Health and Medical Sciences, University of Copenhagen, Copenhagen, Denmark; and [5]Department of Clinical Physiology, Nuclear Medicine and PET, Copenhagen University Hospital Rigshospitalet Blegdamsvej, Copenhagen, Denmark

global CBF by PCM MRI has a number of advantages compared to other techniques. It is completely noninvasive, fast, and can be combined with other noninvasive MRI techniques for absolute quantification of global cerebral metabolic rate of oxygen[7,8] or be used for scaling of regional CBF measured by arterial spin labeling.[9,10] The technique has been used in a number of studies on variation in CBF in healthy individuals[11,12] and in larger population-based studies of aging showing that global CBF decreases with age and that decreased global CBF is associated with accelerated signs of brain aging and increased all-cause mortality.[2,3,6,13–15]

Values of global CBF obtained by PCM MRI in healthy subjects[6,16] are generally in good agreement with accepted textbook CBF values of ~50 mL/100 g/min.[17,18] Previous studies have also shown excellent reproducibility for CBF measurements in vivo[12,16], and shown PCM MRI to be accurate for measuring flow in phantoms[19] and in large vessels.[20]

In order to confidently interpret the physiological significance of these measurements, in vivo validation of the accuracy of PCM MRI for CBF measurements is required. However, comparative studies with accepted reference methods are generally lacking. For human studies, ^{15}O-H_2O positron emission tomography (PET) is generally considered the best available method for absolute CBF measurements.[9,21–24] One previous study failed to show a correlation of CBF measured by PCM MRI and ^{15}O-H_2O PET, but these measurements were obtained months apart and did not account for a number of important physiological covariates.[16]

The aim of the present study was to validate PCM MRI for measurement of global CBF by same-day measurements of global CBF by PCM MRI and ^{15}O-H_2O PET.

Materials and Methods

Twenty-two healthy males (mean age: 27.4 years, range: 18–40 years) participated in the study. The measurements were obtained as a part of a placebo-controlled, crossover study investigating the effect of erythropoietin on cerebral metabolism. Measurements from PCM MRI have previously been published.[8] In the present analysis only data during placebo treatment are included.

The study was approved by the Danish National Committee on Health Research Ethics (H-4-2012-167) and was conducted according to the Declaration of Helsinki. Written informed consent was obtained from all participants.

General Experimental Setup

All experimental measurements in each subject were performed on the same day. Height and weight were measured at the time of inclusion in the study. After an overnight fast, a short catheter was inserted in the radial artery of the nondominant hand for blood sampling. After the ^{15}O-H_2O PET scans, the subjects had a small meal before being transported to the MRI facility. The PET and MRI scans were performed 2–6 hours apart.

Before the PET scans a venous blood sample was obtained and analyzed for hemoglobin. Arterial blood samples were obtained between the two PET scans and again after the MRI CBF measurement, and analyzed for oxygen saturation (SaO_2), and partial pressures of O_2 (PaO_2) and of CO_2 ($PaCO_2$) using a Radiometer ABL800 Flex system (Radiometer, Copenhagen, Denmark). The arterial blood sample obtained at the MRI session was also analyzed for hemoglobin.

PET

PET scans were performed on a Siemens High Resolution Research Tomograph (HRRT) brain PET scanner (Siemens, Knoxville, TN).[25,26] The scanner had an axial field of view of 25 cm and a near isotropic resolution of 2 mm. During PET scanning the subject's head rested in a foam-cushioned headrest, and a head strap was used to minimize head movement. Initially, a 6-minute transmission scan with a rotating ^{137}Cs single-photon point source was performed for attenuation correction.

Approximately 800 MBq of ^{15}O radiolabeled water (half-life: 123 sec) produced online was injected as a bolus using an Automatic Water Injection System (Scansys Laboratorieteknik, Værløse, Denmark).

Arterial blood sampling was initiated 15 seconds before isotope injection. Emission scans were acquired after injection of intravenous bolus of tracer for 7 minutes in dynamic frames of 1 × 30 seconds, 18 × 5 seconds, 9 × 10 seconds, 10 × 15 seconds, and 2 × 30 seconds. Radioactivity concentration in the arterial blood was continuously measured by an automatic blood sampling system and drawn at 8 mL/min (Allogg ABSS, Mariefred, Sweden). The detectors in the system were cross-calibrated against the PET scanner and the sampling frequency was 2 Hz. The inner diameter of the tube connected to the arterial catheter was 1.2 mm. The clocks of the scanner and sampling system were synchronized.

Two consecutive scans were acquired for each subject with an interval of at least 10 minutes between the two injections to allow for washout and isotope decay.

Scans were reconstructed using 3D-ordered subset expectation maximum and point spread function (3D OSEM-PSF).[27] Each map consisted of 207 image planes in a 256 × 256 matrix with an isotropic voxel size of 1.22 × 1.22 × 1.22 mm^3. All images were corrected for randoms, scatter, attenuation (TXTV method),[28] decay and dead time, and filtered with a 3D Gaussian 5 mm filter.

Postprocessing

Quantitative regional CBF-maps were calculated using a 1-tissue 2-compartment model:

$$\frac{dC_t(t)}{dt} = K_1 C_a(t) - k_2 C_t(t) \quad (1)$$

where C_t is the tissue compartment concentration, C_a is the arterial concentration, K_1 is the influx rate constant, which describes the unidirectional clearance of water from the blood to the tissue in mL/100 g/min, scaled to perfusion by a factor of one when assuming full extraction of water, and k_2 is the efflux rate constant (in min^{-1}). The model also accounts for the contribution to the

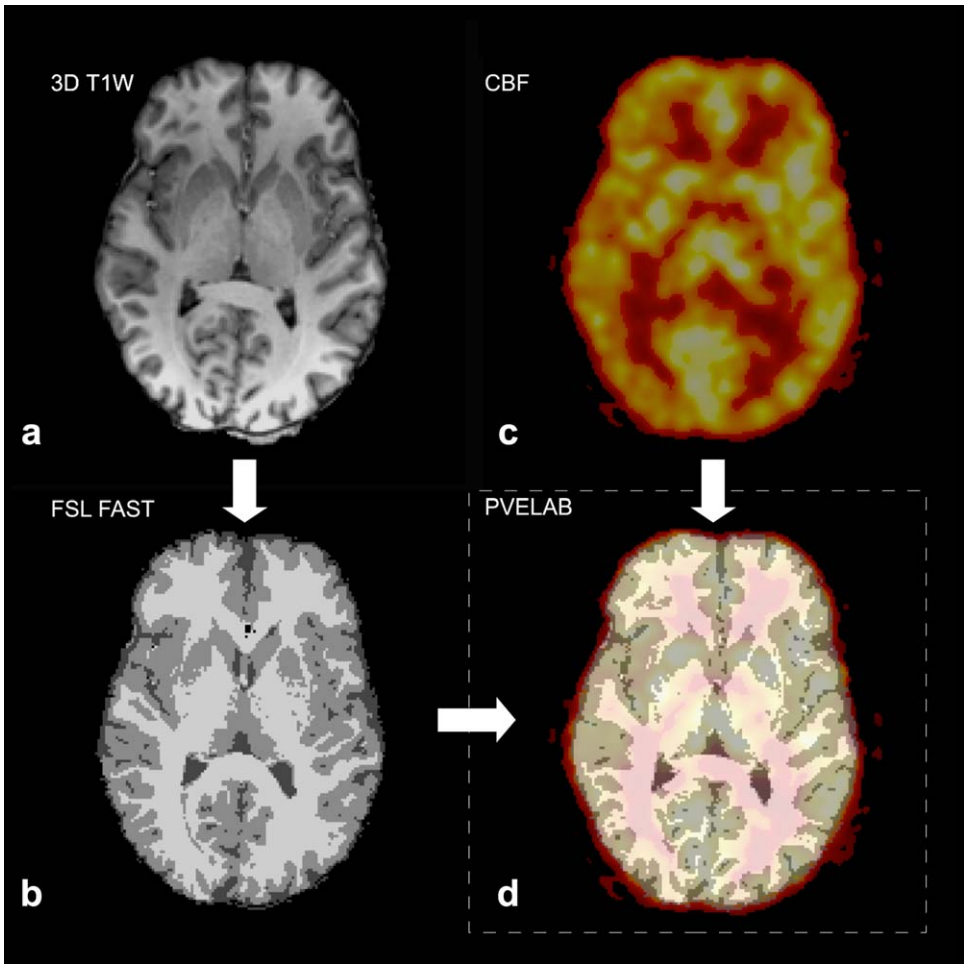

FIGURE 1: Fusion and segmentation of structural MRI and CBF PET maps. The brain extracted 3D T_1-weighted structural MRI scan (a) was segmented into gray and white matter using FSL FAST (b) and coregistered to the CBF PET map (c) of the subject using PVElab software (d). Mean global CBF was calculated as the average of all brain voxels. Note spill-out of PET signal not covered by the brain mask on the fused image.

measured voxel concentration C_{tot} from the vascular volume component vB:

$$C_{tot}(t) = (1 - vB)C_t(t) + vBC_a(t) \quad (2)$$

where C_{tot} is the measured tissue time activity and vB is the blood volume fraction.

The parametric maps were calculated using linear ridge regression with a spatial constraint parameter to increase signal-to-noise ratio (SNR), as described by Zhou et al.[29] The arterial input curves used in modeling were corrected for dead-time, decay, delay, and dispersion. The calculation was done using the software PMOD 3.0 (PMOD Technologies, Zürich, Switzerland).

Using the software PVElab,[30] each regional CBF-map was coregistered to the volume segmented brain tissue mask from the 3D T_1-weighted anatomical MR-scan (Fig. 1), and global CBF was calculated as the mean of all brain voxels.

MRI

FLOW MEASUREMENT. MR scans were performed on a 3T Philips Achieva MRI scanner (Philips Medical Systems, Best, The Netherlands) using a 32-channel phase array head coil. The blood velocity in the carotid and vertebral arteries were measured using a through-plane phase-encoding technique.

The sequence acquires a reference phase image and a velocity sensitive phase image by using a bipolar gradient in the slice-selection direction. By subtracting the velocity sensitive phase image with the reference phase image, a phase-contrast map is calculated. The phase-contrast maps can be scaled to velocity according to the velocity-encoding factor (V_{enc}).

Based on an initial 2D inflow angiogram, the measurement slice was positioned orthogonal to the carotid and vertebral arteries (Fig. 2a). The imaging parameters for the sequence were: field of view (FOV) = 240 × 240 mm^2, voxel size = 0.75 × 0.75 × 8 mm^3, 1 slice, TE = 7.33 msec, TR = 27.63 msec, flip angle = 10°, 10 repeated measures, and total scan time = 1 minute 42 seconds. In order to reduce scan time, cardiac triggering was not applied. When acquiring PCM MRI without cardiac triggering, the *k*-space is random-sampled in an interval including multiple cardiac cycles causing time averaging of the velocity.[19,31] A V_{enc} of 100 cm/s was applied in order to avoid underestimation of flow velocities due to aliasing of the phase at high velocities. When performing measurements without cardiac triggering, potential aliasing from high velocities is not clearly visible because the average velocity is measured.

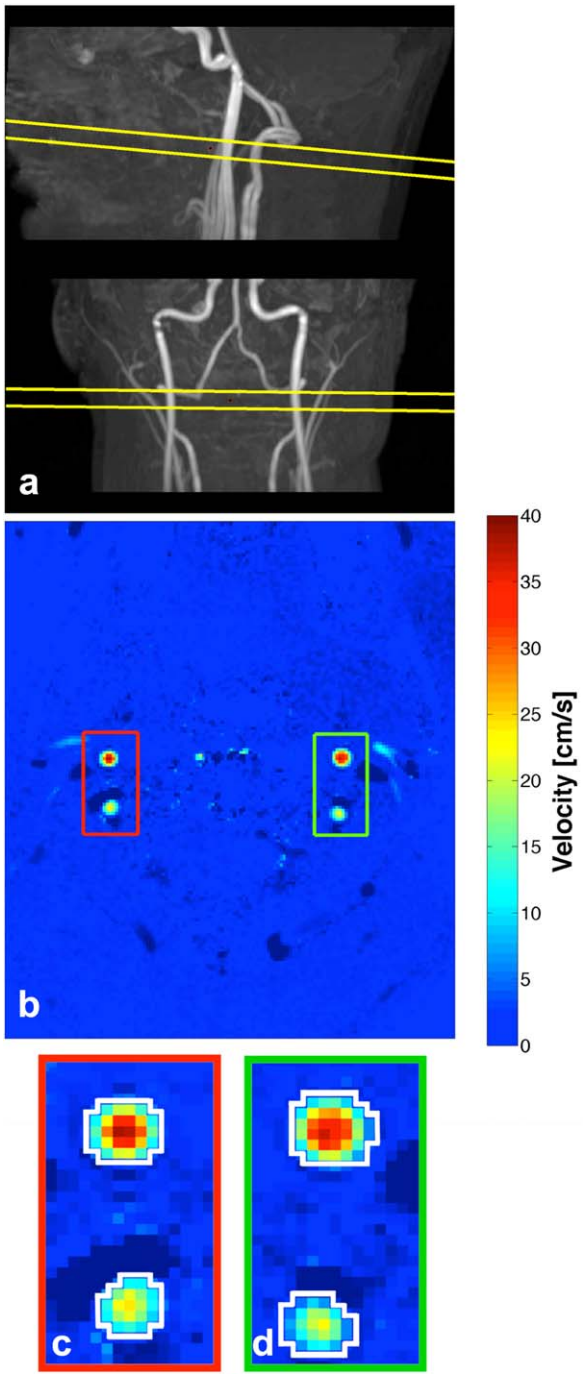

FIGURE 2: Phase-contrast measurements. (a) Example of lateral and anteroposterior maximal intensity projections of the carotid and vertebral arteries with the imaging plane visualized. (b) Example of velocity map measurement perpendicular to the carotids and vertebral arteries. The four arteries are clearly visible. In the lower panel examples of regions of interest (white contours) of the left (c) and right (d) carotid and vertebral arteries are demonstrated.

The V_{enc} was therefore chosen around the upper normal peak velocity values in the internal carotid and vertebral arteries in young subjects while maintaining a reasonable dynamic range.[32]

POSTPROCESSING. The total flow was calculated by measuring the mean velocity and the cross-sectional area of the cerebral arteries by drawing regions of interests (ROI) corresponding to each cerebral artery (Fig. 2b). The ROIs were initially drawn manually on the magnitude image of the first measurement and then copied to the corresponding velocity map. Only voxels with a positive mean velocity were included. ROIs were subsequently copied to the following measurements and inspected for misalignment from possible motion and corrected by moving the ROI if necessary. Cross-sectional area and diameter of the cerebral arteries were calculated from the ROIs. Flow was calculated for each measurement by multiplying mean velocity with the cross-sectional area and integrating over time. The total flow of the four arteries was normalized to whole-brain tissue weight to attain quantitative physiological global CBF values in mL/100 g/min. For comparison with PET, the average of all 10 measurements was used.

ANATOMICAL SCAN. An anatomical scan for segmenting brain tissue was obtained with a 3D T_1-weighted turbo field echo sequence (FOV = 241 × 180 × 165 mm^3, voxel size = 1.09 × 0.81 × 1.1 mm^3, TE = 2.78 msec, TR = 6.9 msec, flip angle = 9°).

The FSL BET and FAST tools (FMRIB Software Library, Oxford University, Oxford, UK)[33] were used to produce a whole-brain tissue mask including cerebral hemispheres (excluding the ventricles), cerebellum, and the brainstem. The mask was inspected (by coauthor M.B.V.) and manually edited if necessary. The same brain volume mask was used for segmentation of the PET scan and for calculation of brain weight assuming a brain tissue density of 1.05 g/mL.[34]

Statistics

For comparison of CBF values, the mean of the 10 repeated PCM MRI measurements and of the two PET scans were used. A paired *t*-test was used to compare mean values of measurements from PET and MRI. Agreement was assessed by linear regression and calculation of Pearson's correlation coefficient (R^2), and by Bland–Altman analysis. Both absolute ($CBF_{PCM} - CBF_{PET}$) and relative ($[CBF_{PCM} - CBF_{PET}]/ CBF_{PET}$) differences were calculated.

As spontaneous fluctuations in $PaCO_2$ have been shown to introduce within-subject variability of CBF measurements,[35,36] the possible influence of $PaCO_2$ fluctuations were investigated by including the difference in $PaCO_2$ ($PaCO2_{PCM} - PaCO2_{PET}$) as a covariate in a multiple regression model with CBF_{PCM} as the dependent variable and CBF_{PET} as the independent variable.

Method precision was assessed as the intrasubject variability derived from a mixed linear model including all repeated measurements of global CBF by each method. Subject was entered as random effect and measurement number as fixed effect in the model. From the mixed linear model within-subject and between-subject variance can be separated. The corresponding within-subject and between-subject coefficients of variation were calculated as the respective standard deviations divided by the mean value of the measurements.

Except where indicated otherwise, all results are reported as mean ± standard deviation.

Results

Results of mean velocity, vessel cross-sectional area, and diameter from PCM measurements are presented in Table 1. Physiological measurements at the two sessions, and brain and body size of participants, are shown in Table 2.

TABLE 1. Results of Phase-Contrast Mapping Measurements

	Flow [mL/min]	Flow fraction [%][a]	Velocity [cm/s]	Area [mm^2]	Diameter [voxels][b]
Right ICA	293.1 ± 53.7	35.4 ± 2.4	21.0 ± 3.1	23.6 ± 4.3	7.3 ± 0.8
Left ICA	292.2 ± 42.0	35.5 ± 2.1	21.0 ± 2.5	23.4 ± 4.0	7.1 ± 0.9
Right VA	102.5 ± 45.9	12.4 ± 4.8	12.4 ± 2.2	13.5 ± 4.7	5.3 ± 1.0
Left VA	135.5 ± 40.5	16.7 ± 4.8	13.8 ± 2.4	16.5 ± 5.0	5.9 ± 0.8
Total	823.3 ± 112.4				

[a]Percentage of total flow, [b]narrowest diameter. ICA, internal carotid artery; VA, vertebral artery.

Mean global CBF was on average 34.9 ± 3.4 mL/100 g/min using ^{15}O-H_2O PET and 57.0 ± 6.8 mL/100 g/min using PCM MRI. Absolute and relative differences between ^{15}O-H_2O PET and PCM MRI were 22.0 ± 5.2 mL/100 g/min and 63.4 ± 14.8%, respectively ($P < 0.0001$ for difference).

Linear regression (Fig. 3a) showed a highly significant positive correlation of PCM MRI and ^{15}O-H_2O PET ($P = 0.0008$, $R^2 = 0.44$). The slope of the regression was higher than one, indicating that the difference between the methods was perfusion-dependent and increased with higher perfusion values. The positive slope of the regression line in the Bland–Altman plot (Fig. 3b) was significantly different from zero ($P = 0.0014$), confirming a systematic perfusion-dependent difference between CBF values obtained by the two methods.

When including $PaCO_2$ difference in the linear model, the effect of $PaCO_2$ difference was near-significantly correlated with PCM CBF (95% confidence interval = [–0.58;10.4], $P = 0.077$) and R^2 increased to 0.53. When comparing the models with and without CO_2-difference by F-test the improvement in fit was shown to be nonsignificant ($P = 0.091$).

Intrasubject variability of global CBF was 6.5% using PCM MRI and 5.7% using PET. The corresponding values of intersubject variability were 11.6% and 8.6%, respectively.

Discussion

The present study compared global CBF values obtained by MRI using PCM and by PET using ^{15}O-H_2O in healthy volunteers. The main finding is that global CBF obtained by PCM MRI is highly correlated with values obtained by ^{15}O-$H_2^{15}O$ PET, thereby confirming the ability of PCM MRI to obtain quantitative measures of global CBF. However, the analysis also demonstrated a systematic relative perfusion-dependent difference between CBF values obtained by the two methods.

The average mean CBF values obtained by the two methods differed in opposite directions from the generally accepted textbook normal global CBF values of 46–50 mL/100 g/min.[17,18] Nevertheless, the values obtained by each method were very similar to those previously reported in healthy subjects,[12,16,37] indicating that the differences more likely reflect general methodological biases rather than the current implementation of the methods or data processing.

The PCM MRI technique has some well-known errors and limitations, primarily related to the limited resolution and the suboptimal measurement geometry of the PCM MRI measurements. First of all, voxels in the periphery of the vessel will contain signal from moving and stationary tissue, causing an underestimation of velocity and overestimation of the cross-sectional area of the vessel. The result of these two opposite effects on flow quantitation has in simulation studies been

TABLE 2. Physiological Measurements and Brain and Body Size

	^{15}O-H_2O PET	PCM MRI	*P*-value for difference
SaO_2 [%]	98.3 ± 0.3	98.1 ± 0.5	0.04
PaO_2 [kPa]	15.6 ± 1.0	14.2 ± 1.3	<0.01
$PaCO_2$ [kPa]	5.6 ± 0.3	5.5 ± 0.5	0.17
Hemoglobin [mmol/L]	8.7 ± 0.6	8.8 ± 0.6	0.71
Brain weight [kg]	1.439 ± 0.114		
Body weight [kg]	81.2 ± 8.9		
Height [cm]	187.5 ± 7.0		

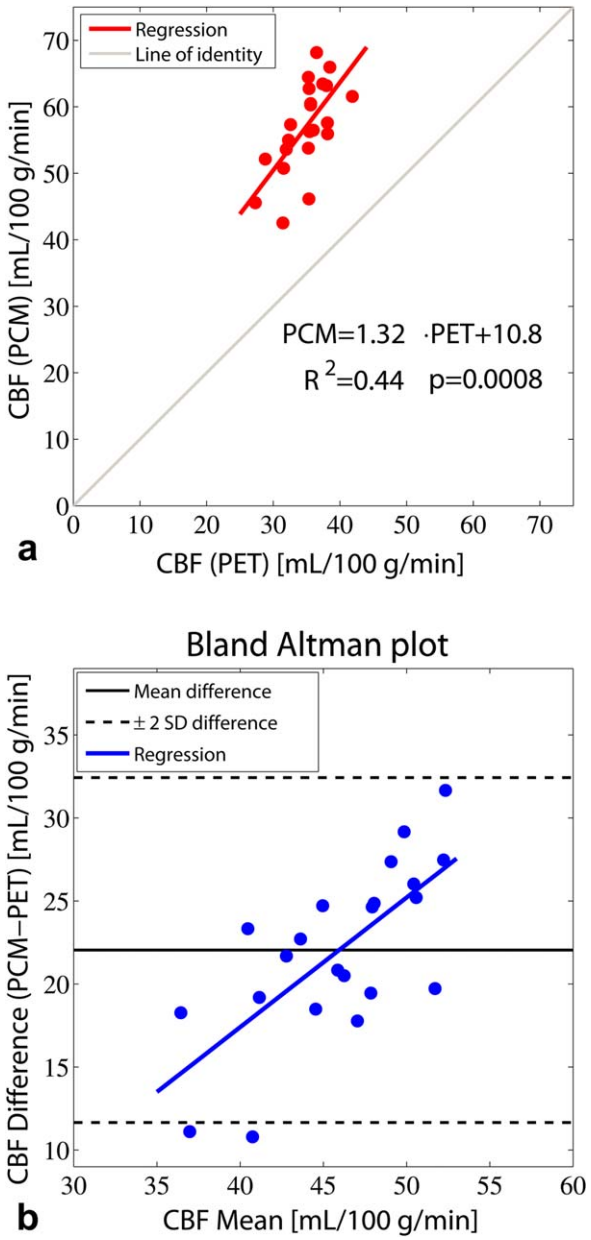

FIGURE 3: Agreement of CBF measurements. (a) Correlation between global cerebral blood flow (CBF) measured by ^{15}O-H_2O PET and phase-contrast mapping (PCM) MRI. (b) Bland–Altman plot showing difference against mean of the methods. Measurement by PCM MRI resulted in higher values compared to ^{15}O-H_2O PET. The positive slope of the regression line of the Bland–Altman plot was significantly different from zero ($P = 0.0014$), indicating a perfusion-dependent relative difference between CBF values obtained by the two methods.

found to be very small if the artery diameter is larger than 5–6 voxels, but will cause overestimation of the flow at smaller relative diameters.[38] In the present study the average diameter of the internal carotid arteries assessed from PCM MRI measurements was 7.2 voxels and of the vertebral arteries 5.6 voxels, corresponding to actual diameters of 5.4 mm and 4.2 mm, respectively. These values are somewhat higher than the corresponding values of 4.8 and 3.3 mm previously reported in young subjects using ultrasound,[39] indicating a possible overestimation of the luminal diameter due to partial volume effect (PVE). Improving in-plane resolution may reduce the partial volume error. Indeed, a recent in vivo study investigating the effects of varying resolution found that PCM flow values acquired at a resolution of 0.7 mm were 13% higher in the vertebral arteries and 6% higher in internal carotid arteries compared to high-resolution imaging at 0.4 mm.[40] However, higher-resolution imaging is associated with prolonged acquisition time and poorer SNR, and the authors of the study concluded that a resolution of 0.5 mm might offer a reasonable trade-off.[40]

Second, a single imaging slice was used to measure velocity in all of the feeding arteries. If the slice is not perpendicular to the vessels, linear velocities will be underestimated and the cross-sectional area will be overestimated. Again, the two effects will tend to balance out, and both simulation and in vivo studies have shown that the effect on flow is negligible if the imaging planes deviate less than 10°, but will cause overestimation at higher degrees of deviation.[38,40] The angle of misalignment on each artery was measured from the angiography images and found to be on average less than 5° on the carotid arteries and less than 6° on the vertebral arteries. The errors related to misalignment are therefore probably very small.

PCM MRI measurements were performed without cardiac triggering in order to reduce scan time. A similar approach has been used in several other studies.[6,15,41] One previous study has shown that nontriggered measurements produced 6% higher flow compared to triggered measurements and was also associated with slightly poorer reproducibility.[12] Other studies, however, have not demonstrated any systematic differences.[19,20,42,43] Nontriggered measurements are less susceptible to irregular or varying heart rate and applying cardiac triggering may prolong acquisition time and potentially cause underestimation of flow, as the entire cardiac cycle is not sampled.

Although often considered a reference standard, the absolute quantification of CBF using ^{15}O-H_2O PET is restricted at high CBF values by the limited water diffusion across the blood–brain barrier. The correct extraction fraction of water depends on the exact tissue measured, the perfusion itself, and interindividual variation, and has been suggested to be in the range of 0.84–0.90 for average global extraction.[44,45] Consequently, when reporting global CBF as the K_1 of the one-tissue model, CBF is underestimated on average by 10–16%.

A further cause of global CBF PET underestimation may be related to a partial volume effect when the low-resolution CBF maps are masked with a high-resolution brain mask, which leads to loss of signal in high-CBF cortical voxels. White matter and cerebrospinal fluid may further contribute to dilution of the cortical signal. A previous ^{15}O-H_2O PET study has shown that a kinetic model incorporating a physiological correction for the segments of the ROI that are not perfused (the nonperfusable tissue fraction) will increase the global CBF value ~17%.[46]

The underestimations of CBF using ^{15}O-H_2O PET due to limited water diffusion and partial volume effects are both perfusion-dependent, causing larger underestimation at high perfusion values. We do not expect the overestimation of flow by PCM MRI to be flow-dependent within the normal perfusion range. The slope of the regression line being larger than one demonstrates this perfusion-dependent underestimation of ^{15}O-H_2O PET.

Method precision of PCM MRI as assessed by the intrasubject coefficient was similar to a previous study that found a corresponding value of 7.4% using a cardiac triggered PCM MRI with similar resolution, also at 3T MRI.[16] This finding thus confirms the very high short-term reproducibility of PCM MRI for measurement of CBF, and does not support the previous report of poorer reproducibility of nontriggered measurements.[12] The intrasubject variability of ^{15}O-H_2O PET CBF measurements was very similar to that of PCM MRI, whereas the intersubject variability was slightly higher using PCM MRI compared to PET. The latter observation may be a consequence of the also slightly higher variability of $PaCO_2$ at the MRI session.

A limitation to the present study is that ^{15}O-H_2O PET and PCM MRI CBF measurements were not performed simultaneously, but separated by a 2–6 hours interval. Spontaneous random variation in CBF could thus contribute to method disagreement. Studies on within-subject variability in CBF are limited and do not separate true physiological fluctuations from methodological imprecision. Including also day-to-day variability, such studies have reported overall within-subject coefficients of variation of between 8.3% and 12.9%, but do not indicate large low-frequency variation in CBF.[18,35,47] As documented by the arterial blood gas and hemoglobin values, the participants were studied in stable, resting conditions at both sessions. We did observe slightly higher PaO_2 and oxygen saturation values during the PET study compared to MRI, but these subtle differences are not likely to influence the CBF measurements and most likely reflect differences in blood sample handling at the two sessions and in calibration of the two blood gas analyzers used. Previous studies have shown that spontaneous fluctuations in $PaCO_2$ is a major source of within-subject variability[35,36] and in the present study residual variability tended to decrease when accounting also for changes in $PaCO_2$.

Finally, changes in CBF and cerebral metabolism from circadian cycle variation may also have contributed to method disagreement and residual variation.[41,48] Such effects cannot be assessed from the present study, but the awake-state circadian changes are relatively small and cannot account for the large offset between ^{15}O-H_2O PET and PCM MRI CBF measurements.

The overall highly significant positive correlation of PCM MRI with ^{15}O-H_2O PET confirms the use of PCM MRI for absolute quantification of global CBF, and thus lends further support for the use of PCM MRI in quantitative studies of cerebral physiology and in population-based studies of cerebrovascular function and brain aging.[6,15,40] In particular, it allows us to more confidently interpret other quantitative physiological MRI techniques relying on accurate measures of global CBF obtained by PCM MRI.[7,10,43] However, it should be stressed that PET and PCM MRI measurements cannot be used interchangeably, as the very large difference will influence all CBF-derived physiological measures directly.

In conclusion, the present study demonstrates that measurement of mean global CBF with PCM MRI and ^{15}O-H_2O PET are highly correlated, thereby validating the use of PCM MRI for quantification of global CBF. The study also showed considerable differences between the two methods, most likely resulting from methodological biases prohibiting interchangeable use of the methods.

Acknowledgments

Contract grant sponsor: Danish Council of Independent Research; contract grant number: 10-094110; Contract grant sponsor: University of Copenhagen; Contract grant sponsor: Lundbeck Foundation through the Center for Neurovascular Signaling (LUCENS)

The authors thank laboratory technician Helle Juhl Simonsen for assistance with blood sampling analysis. The authors also thank nuclear medicine technologist Bente Dall at the Department of Clinical Physiology, Nuclear Medicine and PET for assistance in the ^{15}O-H_2O PET studies, the Cyclotron Unit at the Department of Clinical Physiology, Nuclear Medicine and PET for reliable delivery of ^{15}O-H_2O, and The John and Birthe Meyer Foundation, who donated the HRRT PET scanner to Copenhagen University Hospital Rigshospitalet.

References

1. Kety SS, Schmidt CF. The effects of altered arterial tensions of carbon dioxide and oxygen on cerebral blood flow and cerebral oxygen consumption of normal young men. J Clin Invest 1948;27:484–492.
2. Appelman AP, van der Graaf Y, Vincken KL, et al. Total cerebral blood flow, white matter lesions and brain atrophy: the SMART-MR study. J Cereb Blood Flow Metab 2008;28:633–639.
3. Sabayan B, Grond J Van Der, Westendorp RG, et al. Total cerebral blood flow and mortality in old age A 12-year follow-up study. Neurology 2013;81:1922–1929.
4. Lassen NA. Measurement of cerebral blood flow and metabolism in man. Clin Sci 1982;62:567–572.
5. Wintermark M, Sesay M, Barbier E, et al. Comparative overview of brain perfusion imaging techniques. Stroke 2005;36:83–99.
6. Vernooij MW, van der Lugt A, Ikram MA, et al. Total cerebral blood flow and total brain perfusion in the general population: the Rotterdam Scan Study. J Cereb Blood Flow Metab 2008;28:412–419.
7. Jain V, Langham MC, Wehrli FW. MRI estimation of global brain oxygen consumption rate. J Cereb Blood Flow Metab 2010;30:1598–607.

8. Vestergaard MB, Lindberg U, Aachmann-Andersen NJ, et al. Acute hypoxia increases the cerebral metabolic rate — a magnetic resonance imaging study. J Cereb Blood Flow Metab 2016;36:1046–1058.
9. Zhang K, Herzog H, Mauler J, et al. Comparison of cerebral blood flow acquired by simultaneous [(15)O]water positron emission tomography and arterial spin labeling magnetic resonance imaging. J Cereb Blood Flow Metab 2014;34:1371–1380.
10. Aslan S, Xu F, Wang PL, et al. Estimation of labeling efficiency in pseudo-continuous arterial spin labeling. Magn Reson Med 2011;63:765–771.
11. Dolui S, Wang Z, Wang DJ, et al. Comparison of noninvasive MRI measurements of cerebral blood flow in a large multisite cohort. J Cereb Blood Flow Metab 2016;36:1244–1256.
12. Spilt A, Box FM, van der Geest RJ, et al. Reproducibility of total cerebral blood flow measurements using phase contrast magnetic resonance imaging. J Magn Reson Imaging 2002;16:1–5.
13. Ruitenberg A, den Heijer T, Bakker SLM, et al. Cerebral hypoperfusion and clinical onset of dementia: the Rotterdam Study. Ann Neurol 2005;57:789–794.
14. Wu C, Honarmand AR, Schnell S, et al. Age-related changes of normal cerebral and cardiac blood flow in children and adults aged 7 months to 61 years. J Am Heart Assoc 2016;5:(1).
15. Buijs P, Krabbe-Hartkamp M, Bakker C, et al. Effect of age on cerebral blood flow: Measurement with ungated two-dimensional phase-contrast MR angiography in 250 adults. Radiology 1998;209:667–674.
16. Henriksen OM, Larsson HBW, Hansen AE, Grüner JM, Law I, Rostrup E. Estimation of intersubject variability of cerebral blood flow measurements using MRI and positron emission tomography. J Magn Reson Imaging 2012;35:1290–1299.
17. Lassen NA. Normal average value of cerebral blood flow in younger adults is 50 ml/100 g/min. J Cereb Blood Flow Metab 1985;5:347–349.
18. Madsen PL, Holm S, Herning M, Lassen NA. Average blood-flow and oxygen-uptake in the human brain during resting wakefulness — a critical-appraisal of the Kety-Schmidt technique. J Cereb Blood Flow Metab 1993;13:646–655.
19. Bakker CJG, Kouwenhoven M, Hartkamp MJ, Hoogeveen RM, Mali WPTM. Accuracy and precision of time-averaged flow as measured by nontriggered 2D phase-contrast MR angiography, a phantom evaluation. Magn Reson Imaging 1995;13:959–965.
20. Bakker CJG, Hartkamp MJ, Mali WPTM. Measuring blood flow by nontriggered 2D phase-contrast MR angiography. Magn Reson Imaging 1996;14:609–614.
21. Herscovitch P, Markham J, Raichle ME. Brain blood flow measured with intravenous H2(15)O. I. Theory and error analysis. J Nucl Med 1983;24:9:782–789.
22. Raichle ME, Martin WRW, Herscovltch P, Mintun MA, Markham J. Brain blood flow measured with intravenous H2(15)O. II. Implementation and validation. J Nucl Med 1983;24:790–798.
23. Heijtel DFR, Mutsaerts HJMM, Bakker E, et al. Accuracy and precision of pseudo-continuous arterial spin labeling perfusion during baseline and hypercapnia: A head-to-head comparison with 15O H2O positron emission tomography. Neuroimage 2014;92:182–192.
24. Heijtel DFR, Petersen ET, Mutsaerts HJMM, et al. Quantitative agreement between [(15) O]H2 O PET and model free QUASAR MRI-derived cerebral blood flow and arterial blood volume. NMR Biomed 2016;29:519–526.
25. de Jong HWAM, van Velden FHP, Kloet RW, Buijs FL, Boellaard R, Lammertsma AA. Performance evaluation of the ECAT HRRT: an LSO-LYSO double layer high resolution, high sensitivity scanner. Phys Med Biol 2007;52:1505.
26. Wienhard K, Schmand M, Casey ME, et al. The ECAT HRRT: performance and first clinical application of the new high resolution research tomograph. Nucl Sci IEEE Trans 2002;49:104–110.
27. Sureau FC, Reader AJ, Comtat C, et al. Impact of image-space resolution modeling for studies with the high-resolution research tomograph. J Nucl Med 2008;49:1000–1008.
28. Keller SH, Svarer C, Sibomana M. Attenuation correction for the HRRT PET-scanner using transmission scatter correction and total variation regularization. IEEE Trans Med Imaging 2013;32:1611–1621.
29. Zhou Y, Huang SC, Bergsneider M. Linear ridge regression with spatial constraint for generation of parametric images in dynamic positron emission tomography studies. IEEE Trans Nucl Sci 2001;48:125–130.
30. Svarer C, Madsen K, Hasselbalch SG, et al. MR-based automatic delineation of volumes of interest in human brain PET images using probability maps. Neuroimage 2005;24:969–979.
31. Hangiandreou NJ, Rossman PJ, Riederer SJ. Analysis of MR phase-contrast measurements of pulsatile velocity waveforms. J Magn Reson Imaging 1993;3:387–394.
32. Harloff A, Zech T, Wegent F, Strecker C, Weiller C, Markl M. Comparison of blood flow velocity quantification by 4D flow MR imaging with ultrasound at the carotid bifurcation. AJNR Am J Neuroradiol 2014;34:1407–1413.
33. Jenkinson M, Beckmann CF, Behrens TEJ, Woolrich MW, Smith SM. Fsl. Neuroimage 2012;62:782–790.
34. Torack RM, Alcala H, Gado M, Burton R. Correlative assay of computerized cranial tomography (CCT), water content and specific gravity in normal and pathological postmortem brain. J Neuropathol Exp Neurol 1976;35:385–392.
35. Henriksen OM, Kruuse C, Olesen J, et al. Sources of variability of resting cerebral blood flow in healthy subjects: a study using (133)Xe SPECT measurements. J Cereb Blood Flow Metab 2013;33:1–6.
36. Wise RG, Ide K, Poulin MJ, Tracey I. Resting fluctuations in arterial carbon dioxide induce significant low frequency variations in BOLD signal. Neuroimage 2004;21:1652–1664.
37. Coles JP, Fryer TD, Bradley PG, et al. Intersubject variability and reproducibility of 15O PET studies. J Cereb Blood Flow Metab 2006;26:48–57.
38. Tang C, Blatter DD, Parker DL. Accuracy of phase-contrast flow measurements in the presence of partial-volume effects. J Magn Reson Imaging 1993;3:377–385.
39. Scheel P, Ruge C, Schöning M. Flow velocity and flow volume measurements in the extracranial carotid and vertebral arteries in healthy adults: reference data and the effects of age. Ultrasound Med Biol 2000;26:1261–1266.
40. Peng S-L, Su P, Wang F-N, et al. Optimization of phase-contrast MRI for the quantification of whole-brain cerebral blood flow. J Magn Reson Imaging 2015;1126–1133.
41. Peng S-L, Dumas JA, Park DC, et al. Age-related increase of resting metabolic rate in the human brain. Neuroimage 2014;98:176–183.
42. Enzmann DR, Marks MP, Pelc NJ. Comparison of cerebral artery blood flow measurements with gated cine and ungated phase-contrast techniques. J Magn Reson Imaging 1993;3:705–712.
43. Xu F, Ge Y, Lu H. Noninvasive quantification of whole-brain cerebral metabolic rate of oxygen (CMRO2) by MRI. Magn Reson Med 2009;62:141–148.
44. Herscovitch P, Raichle ME, Kilbourn MR, Welch MJ. Positron emission tomographic measurement of cerebral blood flow and permeability-surface area product of water using [15O]water and [11C]butanol. J Cereb Blood Flow Metab 1987;7:527–542.
45. Paulson OB, Hertz MM, Bolwig TG, Lassen NA. Filtration and diffusion of water across the blood-brain barrier in man. Microvasc Res 1977;13:113–123.
46. Law I, Iida H, Holm S, et al. Quantitation of regional cerebral blood flow corrected for partial volume effect using O-15 water and PET: II. Normal values and gray matter blood flow response to visual activation. J Cereb Blood Flow Metab 2000;20:1252–1263.
47. Petersen ET, Mouridsen K, Golay X. The QUASAR reproducibility study, Part II: Results from a multi-center arterial spin labeling test-retest study. Neuroimage 2010;49:104–113.
48. Braun AR, Balkin TJ, Wesenten NJ, et al. Regional cerebral blood flow throughout the sleep-wake cycle. An H2(15)O PET study. Brain 1997;120:1173–1197.